Science Advances
AAAS

Supplementary Materials for

A 10-micrometer-thick nanomesh-reinforced gas-permeable hydrogel skin sensor for long-term electrophysiological monitoring

Zongman Zhang *et al.*

Corresponding author: Chunya Wang, chunyawang@cup.edu.cn; Takao Someya, someya@ee.t.u-tokyo.ac.jp; Yan Wang, yan.wang@gtiit.edu.cn

Sci. Adv. **10**, eadj5389 (2024)
DOI: 10.1126/sciadv.adj5389

The PDF file includes:

Other Supplementary Material for this manuscript includes the following:

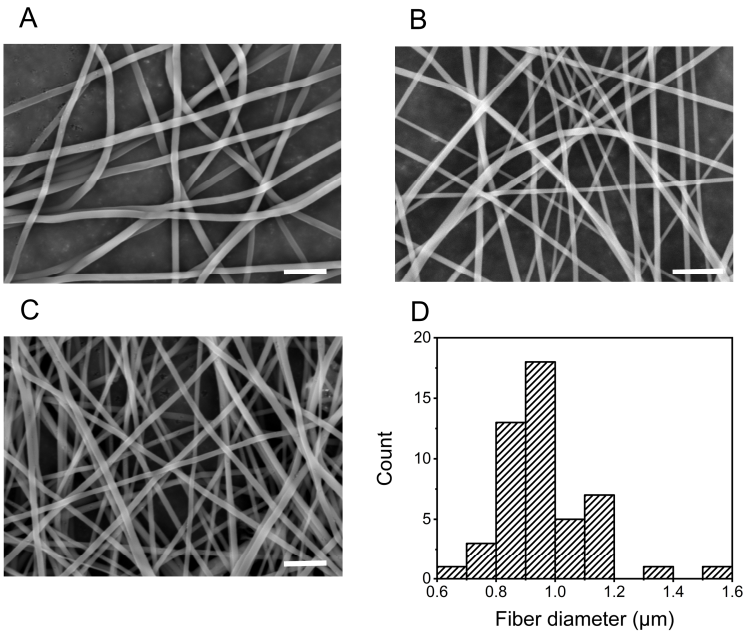

Fig. S1. The morphologies of PU nanomeshes with different densities and diameter distribution. (A to C) PU nanomeshes with densities of (A) 0.3, (B) 0.6, and (C) 1.1 mg cm^{-2}, respectively. Scale bar, 20 μm. **(D)** The statistical data of the diameter distribution obtained from SEM images using image analysis software (image J). N = 50. The average diameter of PU nanomeshes is 0.9 ± 0.1 μm.

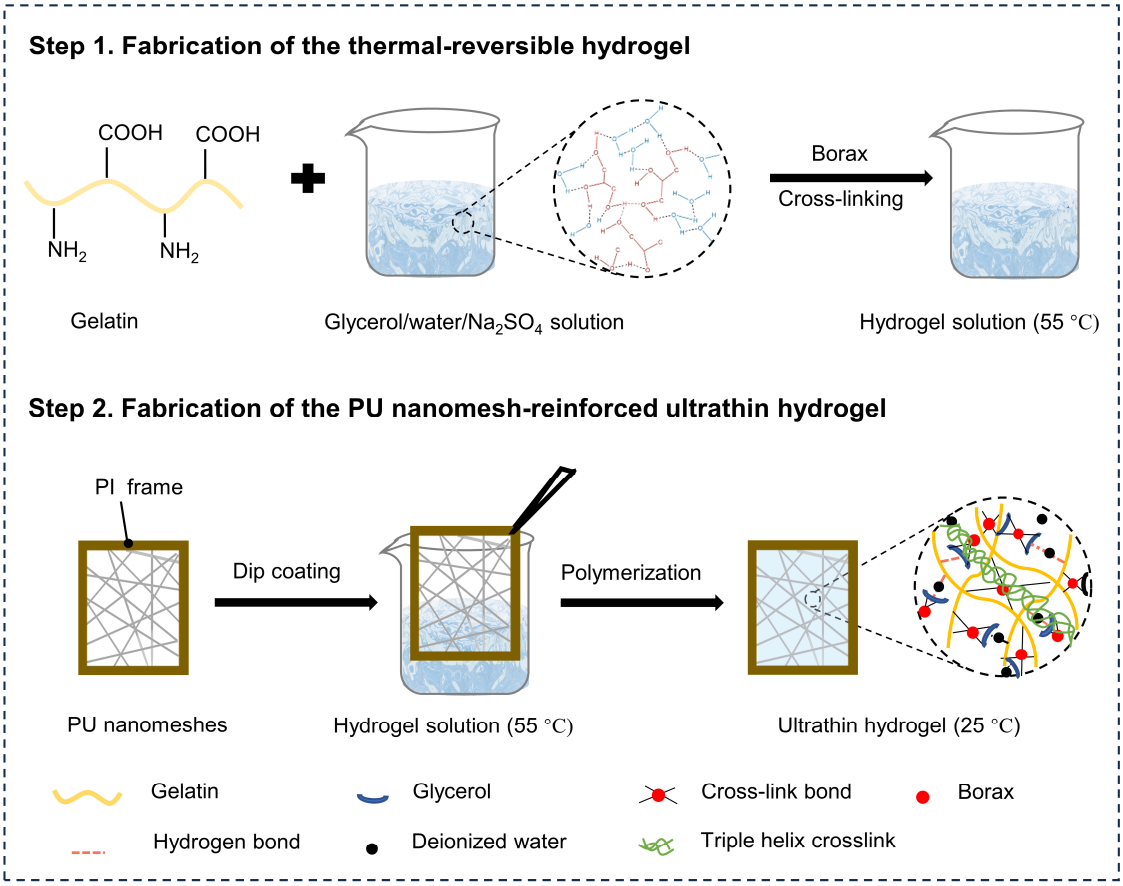

Fig. S2. Schematic illustration of the fabrication process of the ultrathin hydrogels.

The ultrathin-reinforced hydrogel was achieved by dip-coating electrospun nanomeshes (density of 0.3 mg cm^{-2}) into a diluted gelatin hydrogel solution at a high temperature (55–75°C) and then gelating at a physiological temperature or under ambient environment.

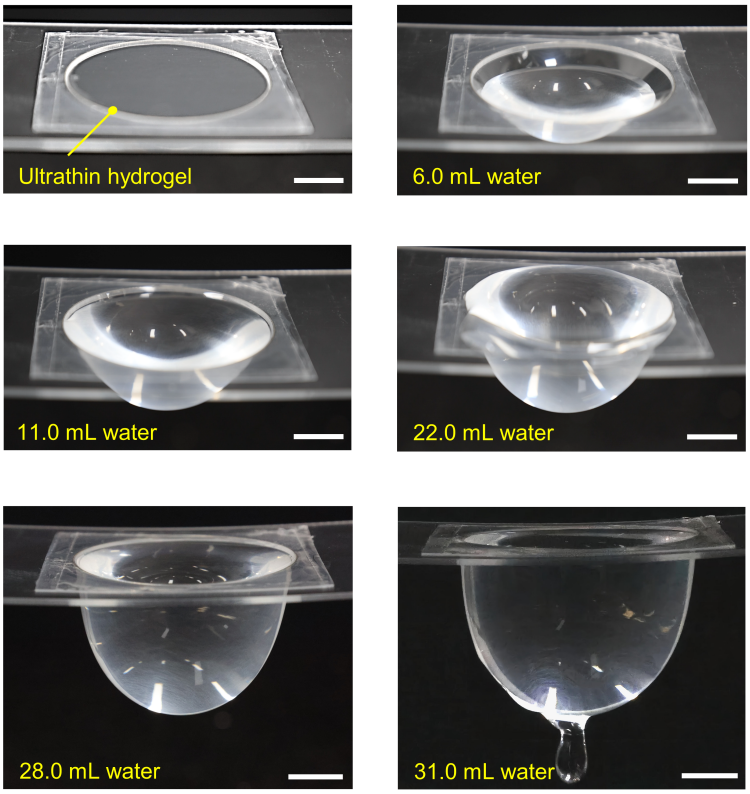

Fig. S3. Mechanical robustness of the ultrathin hydrogels. The ultrathin hydrogel could support water with a volume of 31.0 mL. Scale bar, 1 cm.

In this experiment, the ultrathin hydrogel was fixed on a circular PET window with a diameter of 4 cm, and the water was dripped into the suspended ultrathin hydrogel dropwise.

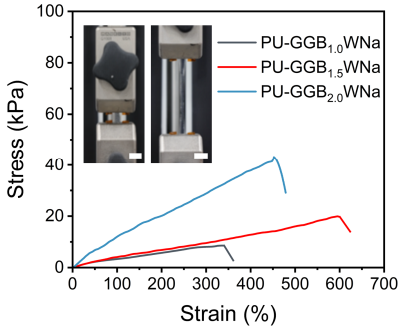

Fig. S4. Tensile test of PU nanomesh-reinforced hydrogels. Tensile stress curves of the PU nanomesh-reinforced hydrogels with different borax content, the insert photographs showing the initial and stretched PU nanomesh-reinforced hydrogels with 1.5 g borax. Scale bar, 1 cm.

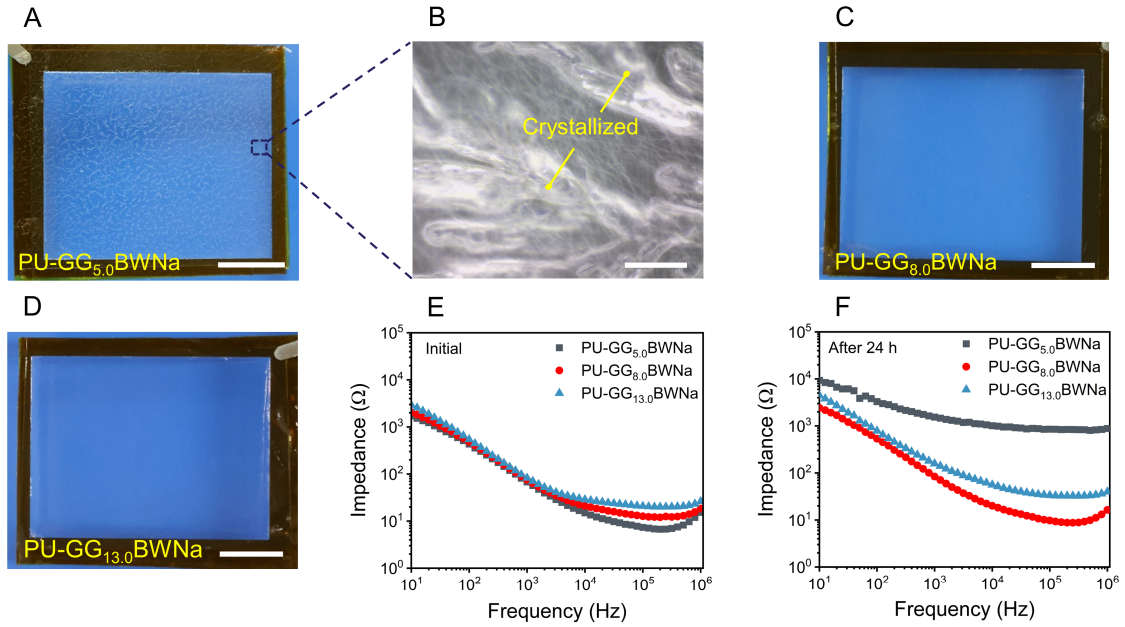

Fig. S5. Influence of glycerol content on anti-drying property and intrinsic impedance of PU nanomesh-reinforced hydrogels. (A) A photograph of PU nanomesh-reinforced hydrogels with glycerol content of 5.0 g (PU-GG$_{5.0}$BWNa) after being stored for 24 h under an ambient environment. Scale bar, 1 cm. **(B)** Microscope image of PU nanomesh-reinforced hydrogels obtained from (A), showing Na_2SO_4 salted out. Scale bar, 1 cm. **(C and D)** Photographs of PU nanomesh-reinforced hydrogels with glycerol content of (C) 8.0 g (PU-GG$_{8.0}$BWNa) and (D) 13.0 g (PU-GG$_{13.0}$BWNa) after being stored for 24 h, respectively. Scale bar, 1 cm. **(E and F)** Intrinsic impedance characterizations of PU nanomesh-reinforced hydrogels with different glycerol content at (E) initial state and (F) after 24 h. Fiber density: 0.3 mg cm^{-2}.

There is a trade-off effect between anti-drying capability and intrinsic impedance. The anti-drying performance was enhanced with the increase of glycerol content, whereas resulting in higher intrinsic impedance. Large amounts of Na_2SO_4 salted out in PU-GG$_{5.0}$BWNa after 24 h due to low glycerol content. Therefore, PU-GG$_{8.0}$BWNa was chosen for further experiments.

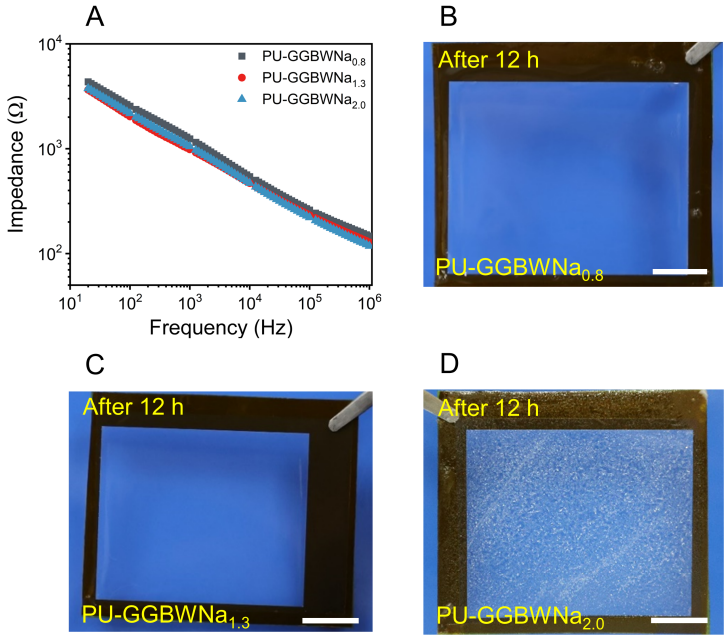

Fig. S6. Influence of Na_2SO_4 content on the intrinsic impedance of PU nanomesh-reinforced hydrogels. (A) The intrinsic impedance curves of PU nanomesh-reinforced hydrogels with different Na_2SO_4 content. **(B to D)** Photographs of the PU nanomesh-reinforced hydrogels with Na_2SO_4 content of (B) 0.8 g, (C) 1.3 g, (D) 2.0 g after being stored for 12 h under an ambient environment, respectively. Scale bar, 1 cm. Fiber density: 0.3 mg cm^{-2}.

The intrinsic impedance of PU nanomesh-reinforced hydrogels decreased with the increase of Na_2SO_4 content (Fig. S6A). However, as the Na_2SO_4 content increased to 2.0 g, a large amount of Na_2SO_4 dissolved out from PU-GGBWN$a_{2.0}$ after being stored for 12 h (Fig. S6B to S6D). Therefore, PU-GGBWN$a_{1.3}$ was chosen for further experiments.

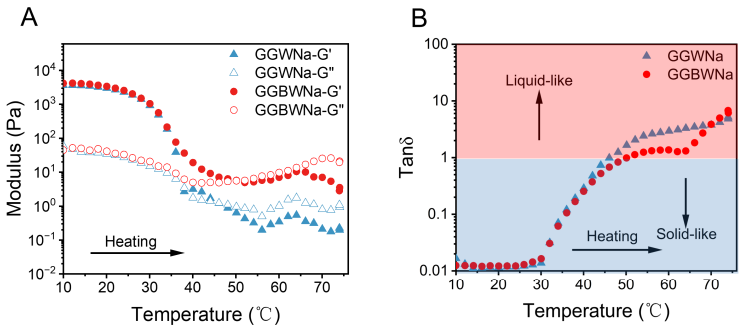

Fig. S7. Rheological test. (A) Rheological characterization of hydrogels solution with different recipes at a temperature sweep from 10 to 75 ℃, showing their transition between viscoelastic gel state and viscous liquid state. **(B)** The corresponding tanδ (G″/G′) calculated from (A).

Fig. S8. A photograph demonstrating the large-scale fabrication capacity of the ultrathin hydrogels. Scale bar, 1 cm.

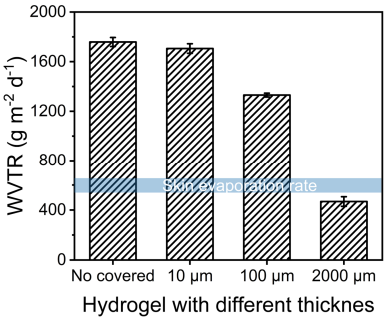

Fig. S9. Comparison of WVTR for PU nanomesh-reinforced hydrogels with different thickness. Fiber density: 0.3 mg cm^{-2}. Error bars represent the SD of the measured values (n = 3).

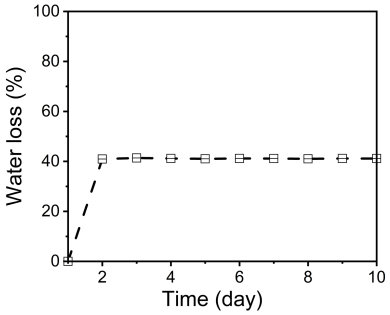

Fig. S10. Anti-drying performance of the ultrathin hydrogels without glycerol.

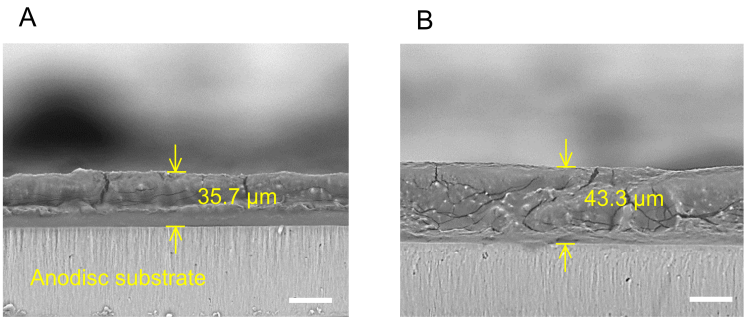

Fig. S11. Cross-sectional SEM images of PU nanomesh-reinforced hydrogels. (A) $PU_{0.6}$-GGBWNa. **(B)** $PU_{1.1}$-GGBWNa. Scale bar, 20 μm.

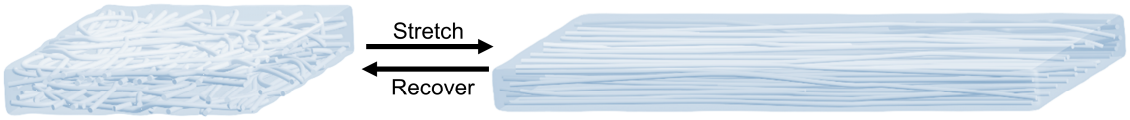

Fig. S12. Schematic illustration of structural changes of the ultrathin hydrogels during reversible stretching.

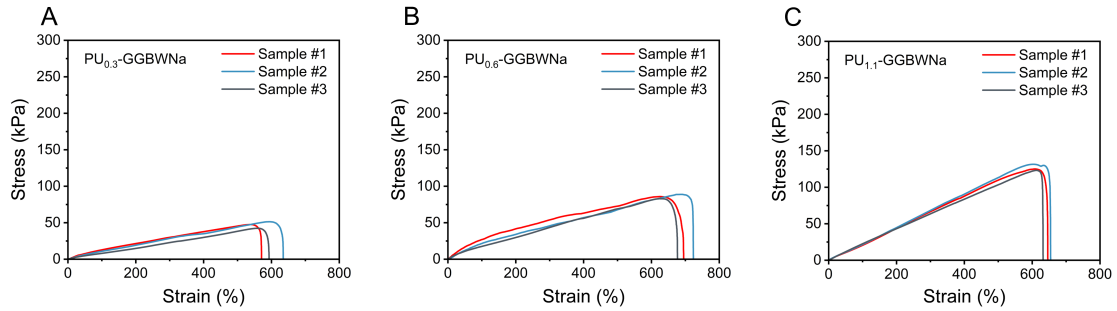

Fig. S13. Tensile stress curves of PU nanomesh-reinforced hydrogels. (A) $PU_{0.3}$-GGBWNa. **(B)** $PU_{0.6}$-GGBWNa. **(C)** $PU_{1.1}$-GGBWNa.

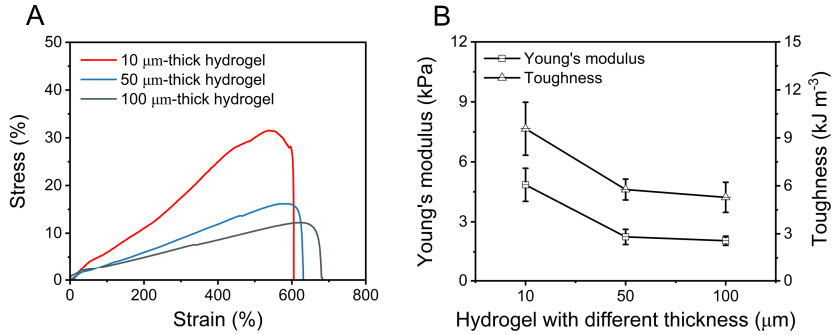

Fig. S14. Mechanical properties of hydrogels of PU nanomesh reinforced hydrogels with different thicknesses. (A) Tensile stress curves of PU nanomesh-reinforced hydrogels with different thicknesses. **(B)** Comparison of Young's modulus and toughness for PU nanomesh-reinforced hydrogels from A. Fiber density: 0.3 mg cm^{-2}. Error bars represent the SD of the measured values (n = 3).

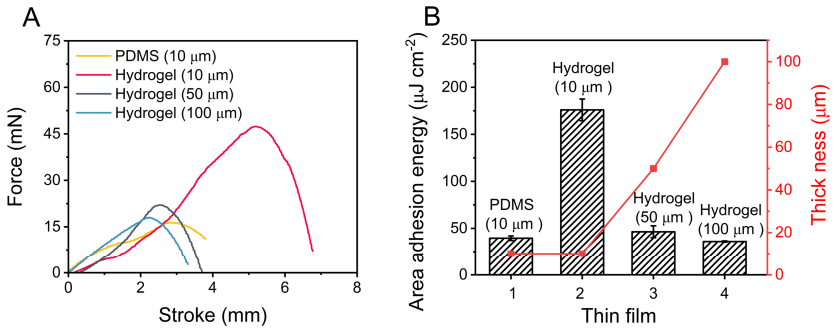

Fig. S15. Comparison of adhesion performance of reinforced hydrogels with different thicknesses and reinforced PDMS films. (A) Force stroke curves of the reinforced hydrogel with different thicknesses and reinforced PDMS films. **(B)** Comparison of the area adhesion energy of the reinforced hydrogel with different thicknesses reinforced PDMS films. Fiber density: 0.3 mg cm^{-2}. Error bars represent the SD of the measured values (n = 3).

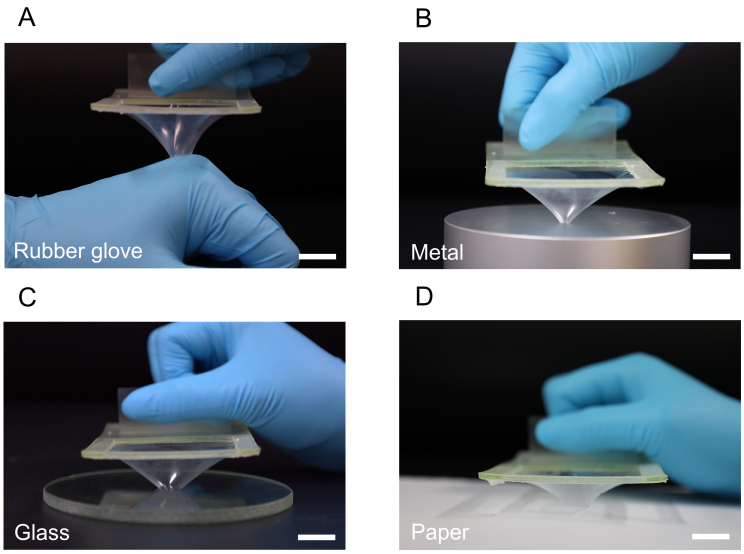

Fig. S16. Photographs of the ultrathin hydrogels attached to different substrates. (A) Attached to rubber glove. **(B)** Attached to metal. **(C)** Attached to glass. **(D)** Attached to paper. Scale bar, 1 cm.

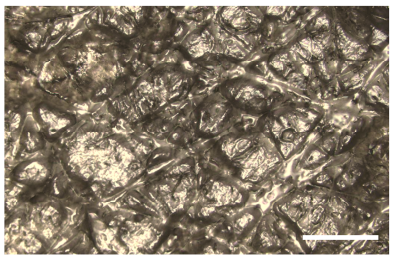

Fig. S17. Optical microscopic image of the peeled-off ultrathin hydrogel surface from the human skin. Scale bar, 500 μm.

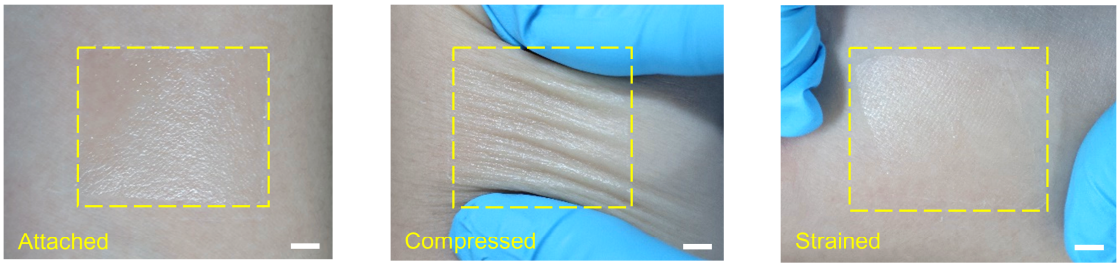

Fig. S18. High skin conformability of the ultrathin hydrogels. The ultrathin hydrogel moves along with natural skin motions during compressing and stretching. Scale bar, 1 cm.

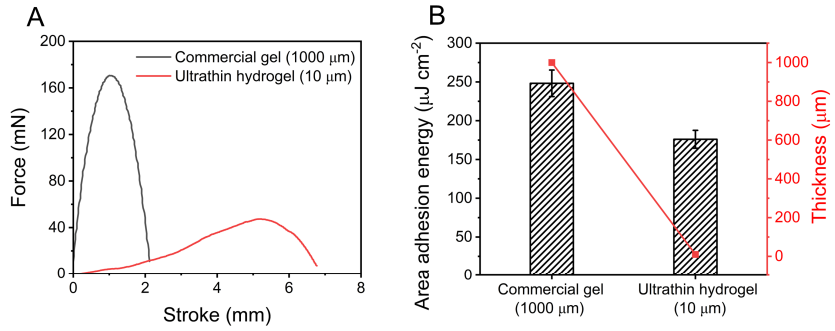

Fig. S19. Adhesion performance of the ultrathin hydrogels and commercial baby-safe ECG gels. (A) Force stroke curves of the ultrathin hydrogels and commercial baby-safe ECG gels. **(B)** Comparison of the area adhesion energy and thickness of the ultrathin hydrogels and commercial baby-safe ECG gels. Error bars represent the SD of the measured values (n = 3).

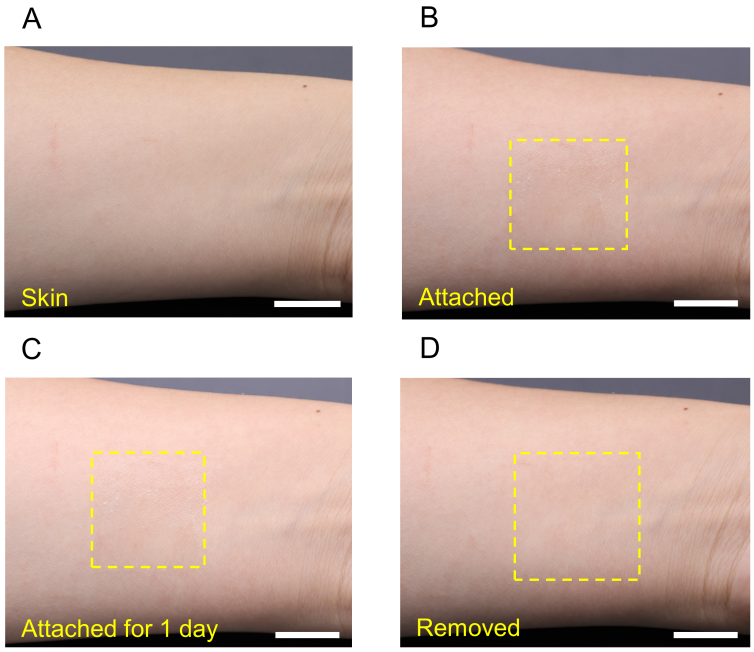

Fig. S20. Evaluation of negative sensations/feelings (e.g., skin irritation, itches, and inflammation) of the ultrathin hydrogel after 24 h of continuous wearing and peeling off. Photographs of **(A)** pristine human skin, **(B)** hydrogel sensor attached to the skin, **(C)** hydrogel attached to the skin for 1 day, and **(D)** after removal.

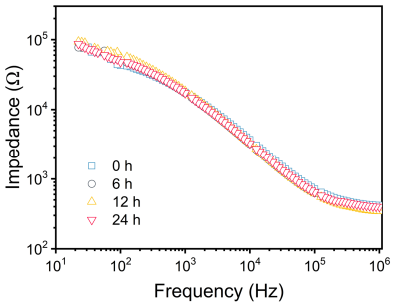

Fig. S21. Skin contact impedance analysis during 24 h of continuous attachment.

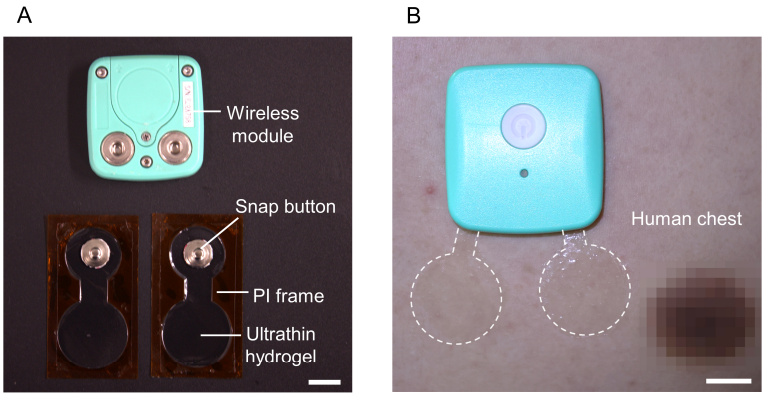

Fig. S22. Photographs of the measurement setup. (A) A photograph demonstrating the wireless module and the design of the ultrathin hydrogel electrode. **(B)** A photograph of the measuring set attached on the human chest. The white dotted line demonstrates the ultrathin hydrogel electrodes. Circular-shaped hydrogel sensors were connected to the contacts of the wireless module that was fixed on the subject's chest. Scale bar, 1 cm.

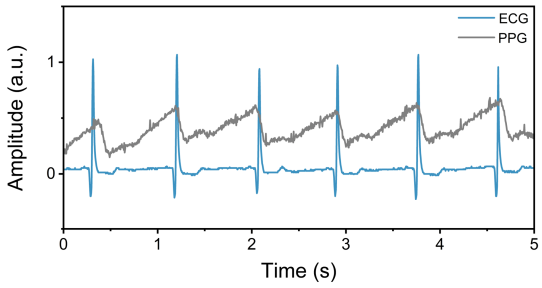

Fig. S23. ECG and PPG signals recorded by the ultrathin hydrogels and commercial PPG ring.

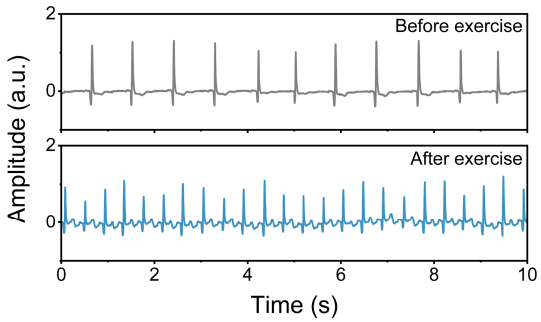

Fig. S24. Wireless ECG recording before (top) and after (bottom) strenuous exercise captured by the ultrathin hydrogels.

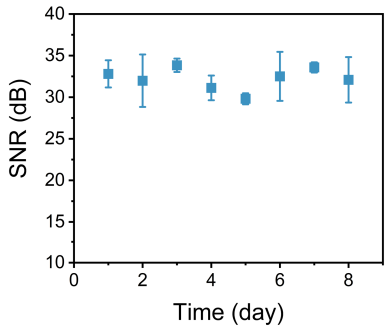

Fig. S25. The SNR of wireless ECG signals continuously monitored by the ultrathin hydrogels for 8 days.

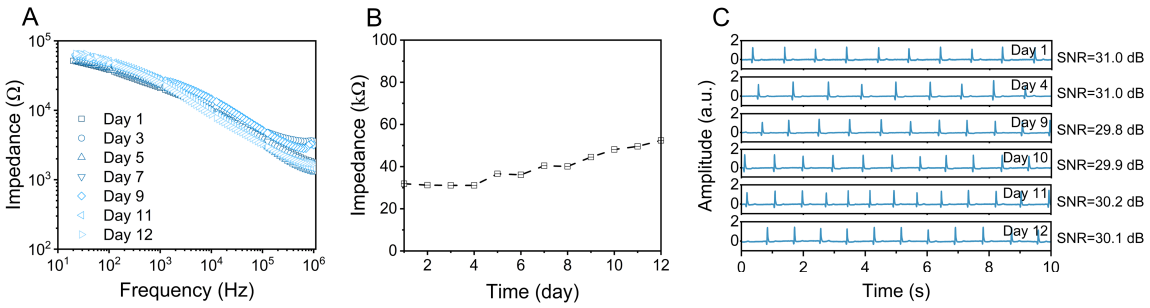

Fig. S26. Long-term skin contact impedance and wireless ECG signals monitoring by the ultrathin hydrogels over 12-day continuous wear under daily life conditions. (A) Skin contact impedance results over 12 days. **(B)** Skin contact impedance at 100 Hz over 12 days. **(C)** ECG signals recorded by the ultrathin hydrogels over 12 days.

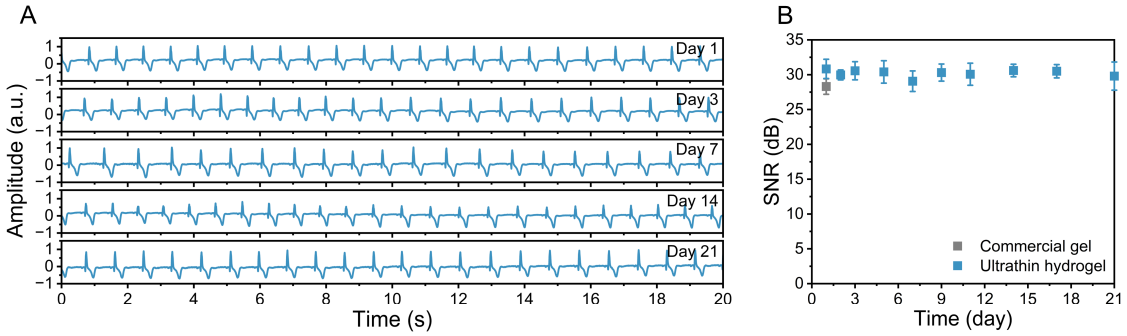

Fig. S27. 21-day ECG signals monitoring by the ultrathin hydrogels. (A) ECG signals recorded by the ultrathin hydrogels after storage for 1, 3, 7. 14, and 21 days, respectively. **(B)** High and stable SNR values by the ultrathin hydrogels after various storage days.

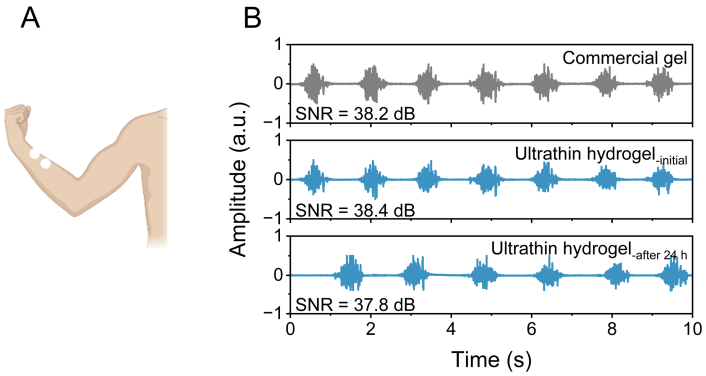

Fig. S28. Long-term, continuous, high-quality EMG monitoring by the ultrathin hydrogels. (A) Schematic illustration of the experimental setup for measuring EMG signals. **(B)** Comparison of EMG signals recorded by commercial gels and ultrathin hydrogels when the subject opened and clenched fist at the initial state and after 24 h of continuous wearing.

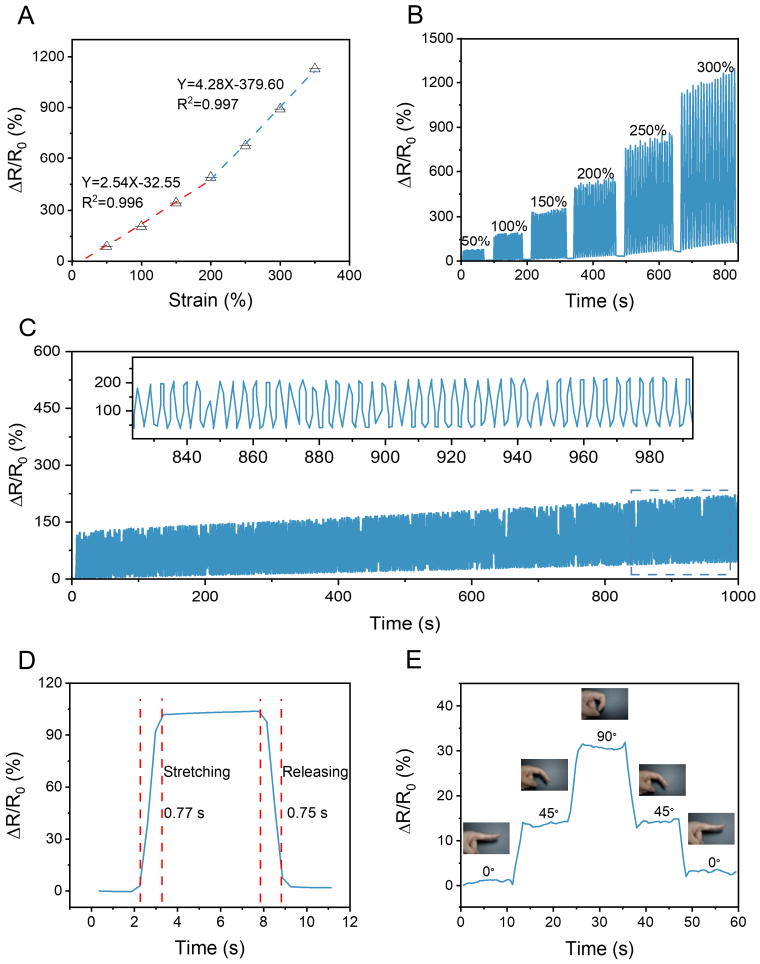

Fig. S29. Strain sensing applications by the ultrathin hydrogels. (A) Relative resistance variation versus applied strain. The slope of the fitted solid line represents the sensitivity of the ultrathin hydrogel. **(B)** Resistance response curves with stepwise increasing tensile strain from 50 to 300% strain. **(C)** Durability test of cyclic stretching/releasing for 500 cycles at 60% strain. **(D)** The response time of the ultrathin hydrogel. **(E)** Relative resistance changes of the ultrathin hydrogel upon bending finger to different angles.

Meanwhile, the ultrathin hydrogel could also be utilized as an on-skin strain gauge. A distinctly nonlinear segmentation trend of the resistance-strain curve is displayed in fig. S29A, suggesting a sensitivity of 2.5 and 4.3 under 0–200% and 200–350% strain, respectively, which are sufficiently large to realize the detection of full body range of motions with high resolution. Fig. S29B presents reproducible dynamic electrical signals during 50–300% strain. The durability test of 500 cyclic stretching and releasing under 60% strain is demonstrated in fig. S29C. Additionally, the ultrathin hydrogel strain gauge exhibits a response time of 0.77 s and a recovery time of 0.75 s (fig. S29D). Finally, real-time finger bending monitoring was demonstrated by the ultrathin hydrogel strain gauge (fig. S29E).

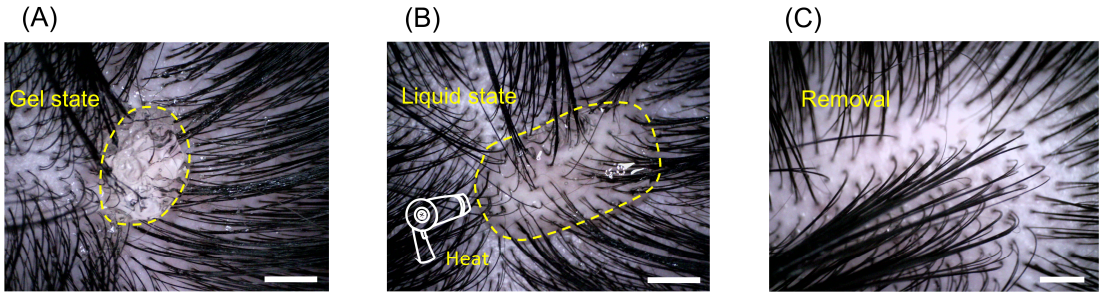

Fig. S30. Photographs demonstrating easy removal of the hydrogel materials from the hairy scalp, taking advantage of the temperature-controlled phase change property. (A) Hydrogels painted on the hairy scalp in a gel state. **(B)** Hydrogel turned into a liquid state after being heated by a hair dryer. **(C)** Clean hairy scalp after hydrogel removal. Scale bar, 1 cm.

Table S1. Comparison of the ultrathin hydrogel with recently reported gas-permeable and/or anti-drying hydrogels in skin bioelectronics on various features, such as thickness, gas permeability, anti-drying, skin adhesion, conductivity, application, and skin-wear period for long-term, continuous health monitoring under daily life conditions.

Materials	Thickness	Permeability	Water loss	Skin adhesion	Stretchability	Young's modulus	Conductivity	Durability	Application (continuous wear)	Ref.
PU nanofiber/PVA/ Glycerol/NaCl	5 μm	-	20% (16 h)	-	~ 300% strain	-	~ 1 Ω/cm^2	-	EMG (-)	22
Polyacrylamide/Sodium alginate/Borax/Tannic acid	10 μm	1890 g m^{-2} d^{-1}	7 days	0.3 J m^{-2} (peel adhesion)	218% strain	540 kPa	-	200% strain, 500 cycles	Flexible optoelectronics (-)	30
Graphene/Polyvinyl alcohol/Polyvinyl pyrrolidone	1000 μm	2.8 kg m^{-2} d^{-1}	-	-	110% strain	112 kPa	-	30% strain, 500 cycles	Motion detection (-)	35
Polyacrylamide/PEDOT:PSS	150 μm	59 % (oxygen penetrating)	10% (with encapsulation)	-	-	-	-	-	Transcutaneous oxygen sensor (-)	6
Au coated nanomesh/ PEDOT:PSS	80 μm	60.7 mg cm^{-2} d^{-1}	-	-	-	-	~ 51.23 Ω/sq	-	ERG (12 h)	36
Gelatin/PPy/Graphene oxide	3000 μm	14 g cm^{-2} h^{-1}	-	-	344% strain	34 kPa	5.25 S/m	-	Motion detection /EMG/ECG (-)	37
Gelatin/Polyvinyl alcohol/Phytic acid	-	220 g m^{-2} d^{-1}	40% (7 days)	-	-	10 ~ 15 kPa	0.13 S/m	10% strain, 200 cycles	Human detection/ECG (-)	38
Gelatin/Yeast/AgNWs	2000 μm	Breathability	-	-	> 300% strain	-	2.4 S/m	-	EMG/ECG (-)	39
Sulfobetaine methacrylate/Polyacrylamide/Polyacrylic acid/LiCl	1000 μm	-	0% (7 days)	-	> 750% strain	-	~ 11 S/m	-	Motion detection (-)	15
Polyacrylic acid/Glycerol/ Polyaniline NFs	1500 μm	-	3.2% (7 days)	~ 12 kPa (peel adhesion)	991% strain	-	-	30% strain, 1000 cycles	Temperature sensor/Motion detection (-)	20
Gelatin/Na_3Cit/ Glycerol/NaCl	800 μm	-	14% (30 days)	-	300% strain	124 kPa	1.6 S/m	-	Motion detection (-)	40
Polyacrylic acid/ Polyacrylamide/Glycerol/Ag flakes	3000 μm	-	18% (60 days)	43.2 J m^{-2} (peel adhesion)	> 500% strain	3.6 kPa	-	-	Motion detection/ECG/EEG (-)	41
Sodium alginate/Polyacrylamide /PEDOT:PSS	2000 μm	-	Less than 50% (3 days)	-	~ 50% strain	-	-	-	EEG (12 h)	27
PU nanomesh/Gelatin/ Glycerol/Borax/Na_2SO_4	10.3 μm	1669.3 g m^{-2} d^{-1}	1% (21 days)	176.8 μJ cm^{-2} (tack adhesion)	696% strain	4.4 kPa	9.3 S/m	60% strain, 500 cycles	ECG/EMG/MCV/EEG/EOG/ABR/VEP/sensor (8 days)	This work

Table S2. Hydrogels recipes with varying components.

	PU nanomeshes (Density)	Gelatin	Sodium sulfate	Borax	Glycerol	Water
GWNa	/	2.5 g	1.3 g	/	/	28.0 mL
GGWNa	/	2.5 g	1.3 g	/	8.0 g	28.0 mL
GGBWNa	/	2.5 g	1.3 g	1.5 g	8.0 g	28.0 mL
PU-GG$_{5.0}$WBNa	0.3 mg/cm^2	2.5 g	1.3 g	1.5 g	5.0 g	28.0 mL
PU-GG$_{8.0}$WBNa	0.3 mg/cm^2	2.5 g	1.3 g	1.5 g	8.0 g	28.0 mL
PU-GG$_{13.0}$WBNa	0.3 mg/cm^2	2.5 g	1.3 g	1.5 g	13.0 g	28.0 mL
PU-GGWB$_{1.0}$Na	0.3 mg/cm^2	2.5 g	1.3 g	1.0 g	8.0 g	28.0 mL
PU-GGWB$_{1.5}$Na	0.3 mg/cm^2	2.5 g	1.3 g	1.5 g	8.0 g	28.0 mL
PU-GGWB$_{2.0}$Na	0.3 mg/cm^2	2.5 g	1.3 g	2.0 g	8.0 g	28.0 mL
PU-GGWBNa$_{0.8}$	0.3 mg/cm^2	2.5 g	0.8 g	1.0 g	8.0 g	28.0 mL
PU-GGWBNa$_{1.3}$	0.3 mg/cm^2	2.5 g	1.3 g	1.5 g	8.0 g	28.0 mL
PU-GGWBNa$_{2.0}$	0.3 mg/cm^2	2.5 g	2.0 g	2.0 g	8.0 g	28.0 mL
PU$_{0.3}$-GGWBNa	0.3 mg/cm^2	2.5 g	1.3 g	1.5 g	8.0 g	28.0 mL
PU$_{0.6}$-GGWBNa	0.6 mg/cm^2	2.5 g	1.3 g	1.5 g	8.0 g	28.0 mL
PU$_{1.1}$-GGWBNa	1.1 mg/cm^2	2.5 g	1.3 g	1.5 g	8.0 g	28.0 mL

Movie captions:

Movie S1. Ultrathin hydrogel supporting liquid.
Movie S2. Dynamic adhesion to the human skin.
Movie S3. Tensile test.
Movie S4. Adhesion evaluation test.
Movie S5. Dynamic compliance to the human skin.
Movie S6. Application of electrical muscle stimulation.